**Department Of Mechanical Engineering**
**Penn State University, University Park, PA 16802**

# SWEPT SHOCK/BOUNDARY LAYER INTERACTION EXPERIMENTS IN SUPPORT OF CFD CODE VALIDATION

*AMES GRANT*

*IN-02-CR*

*110091*

*P_21*

Submitted by:

Prof. G.S. Settles and Y. Lee

## Final Technical Report For
## The Period January 15, 1989 - January 14, 1992

Submitted to:

Dr. C.C. Horstman, Technical Officer
NASA-Ames Research Center, MS 229-1
Experimental Fluid Dynamics Branch
Moffett Field, CA 94035

JULY 1992

Final Technical Report
NASA Grant NAG-2-592
January 15, 1989 - January 14, 1992

**SUMMARY**

Research on the topic of shock wave/turbulent boundary-layer interaction has been carried out under the subject Grant during the past three-year period at the Penn State Gas Dynamics Laboratory. This report describes the experimental research program which provides basic knowledge and establishes new data on heat transfer in swept shock wave/boundary-layer interactions. An equilibrium turbulent boundary-layer on a flat plate is subjected to impingement by swept planar shock waves generated by a sharp fin. Five different interactions with fin angles ranging from 10° to 20° at freestream Mach numbers of 3.0 and 4.0 produce a variety of interaction strengths from weak to very strong. A foil heater generates a uniform heat flux over the flat plate surface and miniature thin-film-resistance sensors mounted on it are used to measure the local surface temperature. The heat convection equation is then solved for the heat transfer distribution within an interaction, yielding a total uncertainty of about $\pm 10\%$. These experimental data are compared with the results of numerical Navier-Stokes solutions which employ a k-$\epsilon$ turbulence model. Finally, a simplified form of the peak heat transfer correlation for fin interactions is suggested.

**Introduction**

The study of shock wave/turbulent boundary-layer interactions is important to the solution of internal and external aerodynamic problems in the design of high-speed vehicles, as well as for the validation of the associated numerical simulations. Despite many previous studies of the overall problem, little knowledge has been gained on *swept* interactions until quite recently, and more extensive experimental work is still needed for a better understanding of the dynamics of such flows.

When an oblique shock wave of sufficient strength impinges upon a solid surface and interacts with the turbulent boundary-layer on that surface, a three-dimensional separated region is generated there. Peak values of surface pressure, skin friction and heat transfer are then observed to occur near the attachment-line of this separated flow. These peak values are of great practical importance in establishing the limits of mean aerothermal loads on high-speed

1

flight vehicles. Also, turbulence and unsteady shock motion result in fluctuations of pressure, skin friction, and heat transfer in such flows, which are sources of serious additional aerothermal loads of an unsteady nature.

With the advent of supercomputers, the computation of such three-dimensional shock/boundary-layer interactions has recently become feasible. Extensive computational studies of sharp-fin-generated swept interactions have been conducted by Horstman[1], Knight[2,3] and Knight et al[4,5] for various interaction strengths using several different turbulence models. These computational results can predict surface pressure distributions, surface flow patterns, and even the gross features of swept interaction flowfields reasonably well. However, it is well known that the prediction of surface pressures is not a definitive test of the turbulence modeling employed in these Computational Fluid Dynamics (CFD) codes. A more definitive test requires that the gradient transport of heat and momentum at the surface be predicted as well. Accurate experimental measurements of skin friction and heat transfer distributions are therefore important for this purpose. Unfortunately, such experimental data of sufficiently high quality and quantity have not generally been available in swept shock/boundary-layer interactions.

The present experimental program has been designed to provide new "benchmark" data of the type required for turbulence modeling, code validation, and physical understanding of these swept interactions. The heat transfer distributions beneath a range of swept interactions are measured, analyzed, and compared with CFD predictions. However, the measurement of accurate, high-spatial-resolution, steady-state heat transfer distributions in swept interactions in a near-adiabatic wind tunnel facility has first required the development of a novel measurement technique, which is also described below.

## Literature Review

Reviews by Settles and Dolling[6,7] cover the progress of research on the swept interaction problem up to 1990. Many studies of the surface properties of such interactions have been made. Some of the more recent of these[8,9] include both surface pressure and skin friction data. Along with these measurements, detailed non-intrusive flowfield studies[10,11] have clarified some previously unanswered questions about swept interaction physics.

In 1977 Neumann and Hayes[12] proposed an empirical correlation for the peak aerodynamic heating in sharp-fin-generated swept interactions. Holden[13] then correlated the

2

results of a number of swept interaction heat transfer experiments with the peak surface-pressure ratio in 1984. Both studies showed that high localized heat transfer occurs near the junction of the fin and the surface. In 1987, Hayashi et al[14] measured heat transfer distributions in swept interactions using a newly-developed thin-film gage. Most recently, Rodi and Dolling[15] measured the surface heat transfer distributions in swept interactions at Mach 5 using steady-state thermopile-type "Schmidt-Boelter" gages.

Although many techniques have been developed by previous investigators to measure aerodynamic heat transfer, no single technique appears to have clearly gained the upper hand. Rather, each technique has its own characteristics which may satisfy certain specific testing requirements. General references[16-19] are available on these conventional heat transfer measurement techniques and instruments. Only the technique of present interest is discussed further here.

**Thin-Film Gages** The development of evaporated metallic-film coating technology in other fields has spawned thin-film gages which are becoming widely used in aerodynamic testing. Because of its high sensitivity and fast response, the thin-film gage is applied in a variety of ways. It can measure highly-transient surface temperatures, it can be used as a calorimeter gage, or it can constitute the sensing element in a multilayer "sandwich" gage. Epstein et al[20] used such gages to measure the heat flux to a transonic turbine, while Hayashi et al[14] first used them to measure heat flux in a shock/boundary layer interaction. Thin-film gages have also been used in transition detection studies (eg Johnson et al[21]).

Although the thin-film technique has versatility, accuracy, and fast response, its fabrication by microlithographic techniques is expensive. The resulting thin-film sensors further need care in handling, annealing to prevent drift, and highly-accurate calibration procedures.

**Resistance Heater Methods** For heat transfer measurements in "cold" facilities it is apparent that external heating or cooling is needed, since a sufficient difference between the surface temperature and the adiabatic wall temperature is critical to the signal-to-noise ratio of the measurement. Such is the case in the present study. Though cooling by way of a circulated refrigerant has been attempted in the past, we have chosen heating by an embedded resistance heater as the simplest means to vary the surface temperature.

The resistance heater method is the most widely-used technique to apply external heating for steady-state heat flux measurements. A heating element inside the surface of a test model

3

generates enough heat to raise the surface temperature significantly. During a test the electrical power input to the heater equals the convective heat transfer from the model surface at steady state. By measuring the local surface temperature and applying the heat convection equation (Newton's law of cooling), the heat transfer coefficient can be calculated.

For example, Simonich and Moffat[22] used a thin gold-film resistance heater to generate a uniform heat flux and cholesteric liquid crystals to sense the resulting surface temperature distribution. Hippensteele et al[23] evaluated commercially-available elements for use in the resistance heater technique. Abuaf et al[24] used a resistance heater/liquid crystal combination to measure the heat transfer distribution in a jet impingement experiment.Eibeck and Eaton[25] used thermocouple measurements beneath a foil heater element to investigate the heat transfer effect of a longitudinal vortex in a turbulent boundary layer.

However, these methods have been used only for relatively-low-speed flows so far. Higher heat generation rates and accurate multipoint surface temperature measurements are needed for high-speed flow experiments. In this study we attempt to combine the above heat transfer measurement technologies to obtain a high-resolution, steady-state measurement technique for high-speed flow in a near-adiabatic wind tunnel facility. Further, in order to obtain high-spatial-resolution data with a modest number of discrete gages, the inherent symmetry of swept interactions must be exploited as well.

**Quasiconical Interaction Structure** The salient feature of the swept sharp-fin interaction (see Fig. 1) is its *quasiconical* symmetry. This has been observed by many investigators and recently confirmed by parametric studies.[8,10] The spanwise interaction growth is found to be essentially conical except for an initial development region or "inception zone" in the immediate vicinity of the juncture of the fin leading edge and the flat plate. The topological features of this quasiconical interaction appear to emanate from a single point, which has been termed the "Virtual Conical Origin" (VCO). Thus a projection along the conical rays of the interaction from the VCO onto a unit sphere reduces the problem to two dimensions, which is a powerful simplification.[7]

Fig. 2 shows such a projection, actually a flowfield map from Ref. 10, as an illustration of the interaction structure in the angular coordinates $\phi$ and $\beta$ of the projection. The swept interaction is seen to consist of a main (inviscid) shock wave which bifurcates into a $\lambda$-foot supported by a separation vortex. The streamtube processed by the $\lambda$-foot turns downward and

impinges upon the flat plate at the rear of the interaction. For a detailed discussion of this structure the reader should consult Ref. 10.

## Experimental Methods

### Wind Tunnel Facility and Test Conditions

The experiments were performed in the Penn State Gas Dynamics Laboratory's Supersonic Wind Tunnel facility, which is an intermittent blowdown tunnel with a test section size of 15 x 17 x 60 *cm.* The facility has a unique variable Mach number capability over the range of Mach 1.5 to 4.0 by way of an asymmetric sliding-block nozzle. A 200 *m,³* 20 *atm* pressure reservoir provides testing times up to 2 minutes at stagnation pressures up to 15 *atm* and a near-ambient stagnation temperature. The experiments described in this paper were performed at nominal freestream Mach numbers of 3 and 4, with corresponding unit Reynolds numbers of 6.8 and $7.0 \times 10^7/m$, respectively.

### Fin Shock Generator

The interaction is generated by an equilibrium, adiabatic flat plate boundary-layer interacting with the swept, planar oblique shock wave generated by an upright, sharp-leading-edge fin at an angle of attack (see Fig. 1). The size of the fin is small enough to avoid blockage of the flow, but large enough to generate a "dimensionless semi-infinite" interaction on the flat plate (see Settles and Dolling[6]). The angle of the fin is controlled by a pneumatic fin-injection mechanism, which is mounted through the tunnel sidewall.

### Turbulent Boundary-Layer

Natural boundary-layer transition typically occurs within 1-2 *cm* of the flat-plate leading edge at the present high Reynolds numbers. Pitot surveys and a wall-wake analysis have established that the flat plate boundary layer is both two-dimensional and in turbulent equilibrium for the range of present test conditions. The parameters of the boundary layer profile at a position 17.8 *cm* downstream of the flat plate leading edge and on the plate centerline are taken as the upstream boundary condition for the present experiments. At freestream Mach numbers 3 and 4, respectively, the boundary-layer thickness is 2.7 and 2.9 *mm,* the displacement thickness is 0.8 and 1.0 *mm,* and the momentum thickness is 0.17 and 0.13 *mm.* A more

complete documentation of the test boundary-layers may be found in Lu.[8]

The turbulent boundary-layer is naturally in a near-adiabatic condition (the ratio of the wall temperature, $T_w$, to the adiabatic wall temperature, $T_{aw}$, is typically 1.03). The resultant thermal potential is quite small, thus requiring the following special means to carry out heat transfer measurements.

## Flat Plate for Heat Transfer Measurements

The flat plate for heat transfer measurements, diagrammed in Fig. 3, is a "sandwich" consisting of a top sheet of RTD (Resistance Temperature Detector) sensors, a foil heater, an insulation board, and a stainless steel supporting plate. A few thermocouples are also distributed inside the insulation board. Heat is generated by the foil heater and the surface temperature distribution is measured by the RTD sensors. The heat convected to the flow equals the total heat generated by the heater ($V^2/R$) minus the heat loss through the insulation board. However, the adiabatic wall temperature is also needed in the calculation of a heat transfer coefficient, and is indirectly measured as described later.

**RTD Surface Temperature Sensors** Custom-made thin-film RTD sensors were vacuum-deposited on a plastic substrate by NASA-Langley Research Center staff using microlithographic fabrication techniques. These thin-film sensors can measure accurate surface temperatures without disruption of the flowfield and have a high frequency response. However, only steady-state measurements are considered in this paper.

Each of the 37 RTD sensors consists of a Nickel-film resistance thermometer of about 1000Å thickness deposited on the 50 $\mu m$ thick Kapton polyimide substrate sheet. The sheet itself is then attached to the flat surface of the foil heater using laminating epoxy. Nickel is chosen as the sensing element because of its relatively-high sensitivity and its excellent adhesion characteristics in thin-film applications. The sensor geometry is the square $1 \times 1$ *mm* serpentine pattern shown in Fig. 4. This pattern maximizes the sensor length in a small surface area, thus producing a high room-temperature resistance (65 $\Omega$), a high signal-to-noise ratio, and effectively a "point" surface temperature measurement. Low-resistance 6 $\mu m$ thick copper-film leads are also deposited from each sensor to the edge of the polyimide sheet. These leads are individually soldered to a 37-conductor coaxial cable, which is then connected to a specially-designed 37-

6

channel signal-conditioner outside the test section.

To utilize the conical nature of the fin interaction, a double-circular-arc distribution of the 37 temperature sensors (at radii of 86.4 $mm$ and 91.4 $mm$ from the fin leading edge) is chosen, as shown in Fig. 5. In terms of the angle $\beta$, defined in Figure 1, these gages are spaced at a 2° angular separation from $\beta = 6°$ to 78° with respect to the freestream for high data resolution.

**Heater** Two types of heating methods are commercially available: the surface resistance heater method and the radiation method. The radiation method utilizes external quartz lamps placed outside the test section and focused upon the model. In general it is a costly and difficult technique. Surface resistance heaters, on the other hand, are widely used because of their relatively low cost and easy application. In this method, the model is heated by a resistance foil imbedded in the model surface.

There are four major requirements for the heater in the present experiment: (1) High heat flux should be generated because of the large convective heat transfer expected in high speed flows. (2) The heat flux should be uniform over the surface of interest. (3) For quick heating during a typical wind tunnel run of about 30 seconds, the thermal mass of the heater should be as small as possible. (4) The surface of the heater should be flat and smooth, since the RTD sheet is mounted on it and exposed to the flow.

Commercially-manufactured "unetched-foil" heaters, as used in a variety of experiments,[22-25] showed quite satisfactory results in terms of uniform heat flux and easy application. However, all these heaters were found to be unsuitable for present purposes because their resistances were too low to generate sufficient heat flux.

For the present study, an Inconel "etched-foil" heater was used instead. This heater is thin and flexible, consisting of an etched-foil resistive element laminated between layers of flexible insulation. It also has a thin aluminum foil over the top surface of the heating element to enhance uniform heating. Custom-made by Minco Products Inc., it is 0.25 $mm$ thick and its room temperature resistance is 21.6 $\Omega$. Using a laminating epoxy, it is "sandwiched" between the RTD sheet and the insulation board (see Figure 3).

**Insulation Board** The heat generated by the heater is transferred to the surroundings by conduction, convection and radiation. In the present experiment radiation is negligible because the temperature is near-ambient. Thus a portion of the heat energy is assumed to be

7

convected to the flow over the plate while the remainder is conducted through the insulation board underlying the heater. A good insulator is needed to minimize this conduction loss. The insulator should further be rigid enough to support the heater during exposure to high-shear flows, and should be machined for surface flatness.

"Rexolite" plastic was chosen for this purpose. It has a low thermal conductivity (0.00035 *Cal/sec/cm/° C*) and also satisfies the stated mechanical requirements. A 4.76 *mm*-thick "Rexolite 1422" sheet was purchased from Almac Plastic Corp. and was machined to size. After attaching the heater and RTD sheet to the insulation board using a "vacuum bagging" technique,[26] the entire assembly was installed on the stainless steel flat plate. Also, to measure the temperature change of the insulation board, three quick-response thermocouples were installed on the top face and two on the bottom face.

## Instrumentation

The RTD sensors, which are at the heart of this experiment, measure temperature by the change of resistance of a sensing element according to a prior calibration. To measure the resistance, it is necessary to provide a constant current flow to the RTD during an experiment. A signal-conditioning instrument was designed and fabricated for this purpose, consisting of 37 sets of constant-current sources (1.5 *mA*), amplifiers, and low-pass-filters for each of the 37 RTD channels.

For the calibration of the RTDs, the internal heater of the plate and a precision thermocouple are used. The heater elevates the temperature of the RTDs and this temperature is measured by the thermocouple. To maintain a uniform temperature over all sensors, a large aluminum block in which the thermocouple is installed is placed on top of the plate and the entire assembly is allowed to reach thermal equilibrium before calibration data are read.

The foil heater is powered through leadwires connected to an AC variable transformer which is capable of an output voltage up to 280 *V* and a current up to 15 *A*. The voltage applied to the heater is recorded during testing.

## Data Acquisition

A LeCroy waveform recorder controlled by a 386-class microcomputer is used for data acquisition. It has 12 channels of high-speed data sampling capability at rates up to 5 *Mhz* and

32 channels of relatively low-speed data sampling at rates up to 5 *Khz*. All these channels utilize 12-bit digitization. The "ASYST" software package is employed for data handling. During experiments, signals from the RTD sensors and thermocouples of the heat transfer model, as well as signals from the wind tunnel stilling chamber, are all simultaneously recorded on the LeCroy system.

## Data Reduction

The present heat transfer measurement technique requires an accurate determination of all the terms in the definition of the Stanton number, $C_h$ :

$$C_h = \frac{h}{\rho_\infty V_\infty c_p} = \frac{q''_{conv}}{\rho_\infty V_\infty c_p (T_w - T_{aw})} \qquad (1)$$

where $h$ is the convective heat transfer coefficient, $\rho_\infty$, $V_\infty$, $c_p$ are the density, velocity and specific heat of the freestream, respectively, $q''_{conv}$ ($W/m^2$) is the heat convected to the flow, $T_w$ is the surface temperature of the flat plate, and $T_{aw}$ is the adiabatic wall temperature.

Except for $T_w$, which is directly measured by the RTD sensors, all terms in the above equation must be determined indirectly from measured values. In particular, the accurate determination of both $q''_{conv}$ and $T_{aw}$ is essential since these parameters principally determine the accuracy of the Stanton number. They are, however, not easy to measure. $T_{aw}$ is never reached during the present brief wind tunnel runs, even on an insulating model. Further, the variation of temperature within the insulation board is quite complex during a run due to changing stagnation temperature and heater voltage, requiring that a special calculation be performed.

**Conduction Loss Calculation** From the measured voltage applied to the foil heater and its resistance, its heat efflux is easily calculated. However, it was already noted that not all of this heat efflux is convected to the flow. There is also a conduction loss through the insulation board which must be determined. $q''_{conv}$ is then calculated by subtracting this conduction loss from the heat efflux produced by the heater.

The conduction loss is calculated using the measured RTD temperature and the bottom temperature of the insulation board by solving the time-dependent 1-D heat diffusion equation with an imbedded heat-source layer:

where $t$ is time, $x$ is depth into the plate measured normal to the top surface of the RTD sheet

$$\frac{\partial T}{\partial t} = \frac{\partial}{\partial x}(D\frac{\partial T}{\partial x}) + \rho c_p \dot{g} \qquad (2)$$

(see Fig. 6), and $D$, $\rho$, and $c_p$ are the thermal diffusivity, density, and specific heat of the multi-layered components of the plate, respectively. Also $\dot{g}$ $(W/m^3)$ is the rate at which heat is generated per unit volume of the foil heater. The measured time-dependent RTD and insulator-bottom temperatures serve as boundary conditions, and a constant-temperature initial condition throughout the plate is both assumed in the solution and forced in the actual experiment by allowing adequate time for thermal equilibration between runs. The numerical solution of Eqn. (2) yields temperature vs. time for 49 nodes within the plate, from which the time-dependent conduction loss to the insulation board, $q''_{loss}$ $(W/m^2)$, is obtained from Fourier's law:

$$q''_{loss} = -k\frac{dT}{dx} \qquad (3)$$

using the first two node temperatures at the top of the insulation board to form the gradient. ($k$ is the thermal conductivity of the insulation board.)

Of course, this procedure accounts only for conduction *normal* to the plate surface. Lateral conduction effects are estimated in Ref. 26 and found to be, at worst, 20% to 30% of the normal conduction, which is itself on the order of 10% of the total heat produced by the heater. Accordingly, no correction has been carried out for lateral conduction.

**Adiabatic Wall Temperature** In the present experiment an accurate evaluation of $T_{aw}$ is a most critical step, since $T_w$ - $T_{aw}$ is relatively small at the location of peak heat transfer in the shock/boundary-layer interaction. Although most previous experimental studies have assumed that $T_{aw}$ is constant beneath such interactions, it is necessary to check that assumption here in order to maintain the accuracy of the present results.

There are two methods generally used to measure $T_{aw}$: the "direct" method and the "indirect" or extrapolation method. The direct method measures $T_{aw}$ directly upon an insulated model after thermal equilibrium is reached.[27-29] However, in most of these cases the required tunnel run time was quite long, which is not possible for the present tests.

Neumann and Hayes[12] discuss the general problem of recovery temperature $(T_{aw})$ measurement and present a classical way to solve it. This method involves making several heat flux measurements at different wall temperatures. Since the heat flux is linear with $T_w$ so long as the heat convection coefficient is constant, a linear fit to the data can be extrapolated to the

10

temperature at which zero heat is convected to the flow, which is identically $T_{aw}$. The present experiments employ this "indirect" method.

**Data Reduction Program** The data reduction program is written in FORTRAN and runs on a 386-class microcomputer. It consists of one main program and two subroutines which accept as input all 42 data channels for 6 different heating rates, a total of 252 data files. The program then calculates the distribution of $C_h$ at 35 different $\beta$-locations of the RTD sensors in the interaction. For each RTD location the calculation procedure is executed in time, with 0.05 *sec* time steps beginning at the start of the wind tunnel run. The calculation procedure is as follows:

1) The heat generated by the heater, $\dot{g}$, is calculated.
2) The 1-D unsteady heat diffusion equation is solved for 49 nodal temperatures in the plate.
3) The heat loss to the insulation board is obtained by solving the conduction equation.
4) From $\dot{g}$, $q''_{heater}$ is determined by multiplying by the surface area of the heater. The heat convected to the flow is then calculated by subtracting the calculated conduction loss from $q''_{heater}$.
5) $T_{aw}$ is calculated by the indirect method just described.
6) Wind tunnel freestream properties are calculated.
7) Finally, mean $C_h$ values are calculated at each $\beta$-location by averaging the values over a 5 *sec* period near the end of the wind tunnel run.


**Error Analysis** The uncertainty of each variable in the above process contributes to the total uncertainty of the final result. As Coleman and Steele[30] suggest, the total uncertainty of the present measurements is determined by calculating and combining the "root-sum-squares" of the uncertainties of each variable in the data reduction equation. This calculation indicates a maximum total uncertainty in $C_h$ of about $\pm 10\%$ for all 5 present interaction cases. This accuracy level is believed to qualify the present results as "benchmark" data for code validation and turbulence modeling purposes. The error bars shown on selected points in the upcoming figures reflect this uncertainty estimate.


## Computational Methods

The governing equations describing the shock/-boundary-layer interaction flowfield are the

11

compressible 3-D Navier-Stokes equations using mass-averaged variables in strong conservation form. These equations are listed in Ref. 31. Their restrictions include the calorically-perfect-gas assumption, the Sutherland viscosity law, and zero bulk viscosity. Turbulence closure is achieved with a two-equation eddy-viscosity ($k$-$\epsilon$) model using the Jones-Launder low-Reynolds-number terms.[32] Further details of the boundary conditions and algorithm used here are given by Knight $et$ $al.$[33] and Horstman.[1]

The computational domain extends from a prescribed upstream boundary where an equilibrium turbulent boundary-layer is generated (matching the experimental data) to a point well downstream of the interaction. Within this domain the grid is generated so as to take advantage of the experimentally-observed quasiconical flowfield. In the $x$-$z$ (horizontal) plane the grid is developed using a family of rays originating from a virtual conical origin slightly upstream of the fin leading edge. Ahead of the interaction these rays are replaced by lines of constant $z$ (spanwise direction). In the $x$ (streamwise) direction, constant spacing is used. In the $y$ (vertical) direction a variable spacing is used, concentrating most of the points within the boundary layer. The maximum value of $y^+$ for the first grid point is 0.1 in the interaction region. The resulting grid spacing in the $x$ and $z$ directions is approximately half the incoming boundary-layer thickness. The total computational domain encompasses 64x40x64 grid points in the $x$, $y$, and $z$ directions, respectively.

To calculate $C_h$, two separate computations are made for each test case. The heat convected to the flow is determined from the first computation, in which $T_w$ is set at 22° C above the stagnation temperature. A second computation is then made in order to find $T_{aw}$, where the heat convected to the flow is set to zero as a boundary condition. $C_h$ is then calculated using Eqn. (1), just as in the case of the experimental data. Ideally, in fact, six computations should be done, just as six experiments are carried out at different heating rates, for better accuracy. However, since each solution requires 25 hours on the NASA-Ames Cray YMP supercomputer, such an approach is not realistic.

### Results and Discussion

Fig. 7 shows the time variations of $T_w$ at two representative RTD sensor locations ($\beta = 64°$, located outside the interaction, and $\beta = 20.8°$, located at the point of peak heat transfer) in the Mach 4, $\alpha = 16°$ fin interaction $without$ heating. Fig. 8 shows the corresponding case $with$

12

heating, where the two wall temperatures are elevated well above the adiabatic wall temperature. The "knees" in the variation of the wall temperatures in Fig. 8 (at 12.5 *sec*) are due to a deliberate abrupt change of the heating rate during the run, which was required to raise the plate temperature rapidly at the beginning of the run in order to save testing time. The tunnel stagnation and adiabatic wall temperature variations (calculated under the assumption that the recovery factor equals 0.89 based on many measurements of high-speed turbulent boundary-layers) are also shown for a comparison.

Fig. 9 shows a comparison of the computed conduction loss through the insulation board at the same two sensor locations ($\beta=64.0°$ and $20.8°$) for the same interaction. Similar "knees" at 12.5 *sec* are also seen here. At the location of peak heat transfer ($\beta=20.8°$) the conduction loss is actually negative at the end of the tunnel run because heat is so strongly convected to the flow there.

In Fig. 10 the calculation of the adiabatic wall temperature using the "indirect" extrapolation method described earlier is illustrated for the case of a sensor located in the flat plate boundary-layer at $M_\infty=4.0$. Six different heating rates show the expected linear variation with wall temperature which, upon extrapolation, yields a flat-plate recovery factor of 0.90. This is sufficiently close to the value of 0.89 which is expected for compressible turbulent boundary-layers. A 95% confidence interval is also shown on the data in Fig. 10, which is used for the error analysis[26,30] of the measurements.

In order to check the accuracy of the present heat transfer technique, a comparison of the experimental results for the flat plate case with a numerical calculation using an eddy-viscosity boundary-layer code[34] was carried out. The results show that the raw $C_{h\infty}$ data from the experiments generally agree with the CFD calculation within 15% except at certain particular RTD locations. These particular exceptions, at which fixed errors arise due to a slight local nonuniformity of the foil heater, are corrected by way of a calibration process.

## Heat Transfer Distributions

Figs. 11 to 15 show the normalized heat transfer distributions, $C_h/C_{h\infty}$, vs. the angle $\beta$ for 5 different swept shock wave/boundary-layer interactions ranging from weak to strong. Here, $\beta_{pr}$, $\beta_{ss}$, $\beta_{ps}$, and $\beta_{ui}$ represent the angular locations of primary attachment, secondary separation, primary separation and upstream influence, respectively, in spherical polar coordinates centered

13

at the fin leading edge for simplicity. For the cases of $M_\infty=3.0$, $\alpha=16°$, and $M_\infty=4.0$, $\alpha=16°$ and $20°$, numerical solutions are also available and are shown along with the data.

The weakest interaction, $M_\infty=3.0$, $\alpha=10°$ shown in Fig. 11, displays a relatively featureless rise in heat transfer from the primary flow separation line to a peak at the primary attachment line, where $C_h$ reaches about twice its flat-plate value. In the $M_\infty=3.0$, $\alpha=16°$ case of Fig. 12 similar features are seen, though the rise now begins at the secondary separation line and reaches a peak of $C_h/C_{h\infty}=3.2$. The CFD solution in this case is in very good agreement with the experimental data except in the vicinity of $\beta_{ss}$, where a "dip" below the flat-plate level is predicted but not observed in the data.

Fig. 13 next shows the measured heat transfer distribution for the $M_\infty=3.0$, $\alpha=20°$ interaction. The rise begins at primary separation as before, but a small local maximum is noted around $\beta=41°$, perhaps associated with the incipient secondary separation which occurs slightly upstream of that location. The rise then continues to a maximum at the primary attachment line, where four times the flat-plate heat transfer level is observed.

Fig. 14, for the $M_\infty=4.0$, $\alpha=16°$ interaction, shows a case of very similar interaction strength, since the Mach number normal to the undisturbed oblique shock wave in these two cases is 1.8 and 1.9, respectively. Indeed, the observed peak heat transfer levels in Figs. 13 and 14 are almost the same. However, in the latter case the CFD solution underestimates the peak level by some 20% for unknown reasons.

Finally, Fig. 15 shows the results of the strongest interaction tested here: $M_\infty=4.0$, $\alpha=20°$. As in Fig. 13, a small local maximum in heat transfer is seen in the vicinity of $\beta_{ss}$. Otherwise the data rise to a peak value of $C_h/C_{h\infty}=5.1$ at the primary attachment line. This level is well-predicted by the CFD solution, although its $\beta$-location is offset slightly, due to the fact that the computed boundary layer on the fin itself is too thick.

In summary, the salient feature of the present results is that peak heating occurs on the primary attachment line of these swept interactions. The peak heating level also rises monotonically with normal Mach number $M_n$ (a first-order interaction strength parameter[10]), as shown by both the experimental data and the CFD solutions.

## Peak Heating Correlation

The peak heating correlation of Neumann and Hayes[12] is a function of both normal Mach

number and position $x/\delta$ downstream of the leading-edge of the fin. Their work was done before the quasiconical nature of the fin interaction was generally recognized. If it is assumed that $C_h$ asymptotes to a constant value along a concial ray outside the interaction inception zone, as is shown experimentally by Rodi and Dolling,[15] then a much-simpler data correlation can be posed in terms of $C_{h,peak}/C_{h\infty}$ vs. $M_n$ only. This correlation is demonstrated in the graph of Fig. 16.

In Fig. 16 the present data are shown with solid symbols. Other available data are shown by open symbols, including those of Rodi and Dolling,[15] Law[35] (based on data actually measured by R. D. Neumann), and Oskam.[36] Taken together, these data approximately describe a linear relationship within their overall scatter. The equation of the line shown in Fig. 16 is:

$$\frac{C_{h,peak}}{C_{h\infty}} = 2.8M_n \qquad (4)$$

This relationship is hereby proposed as a simple empirical guide for peak heating in sharp-fin-generated interactions with turbulent boundary layers *outboard of the inception zone near the fin leading edge*. No such simple relationship is possible inside the inception zone, though the prior work of Neumann and Hayes[12] indicates lower peak heating levels there. Eqn. (4) above would then yield a conservative estimate for practical purposes.

The data shown in Fig. 16, from which Eqn. (4) is derived, are chosen from the available literature because their accuracy is reasonably documented and because it can be demonstrated that they were obtained outside the interaction inception zone. Heat transfer data at freestream Mach numbers higher than 6 are available (*eg* Ref. 37), but unfortunately this latter condition cannot be satisfied. The reason for this appears to be that very high Reynolds numbers, and consequently long distances downstream of a flat-plate leading edge, are generally required to produce an equilibrium turbulent boundary-layer in hypersonic wind tunnel testing. For this reason such a boundary-layer tends to be comparatively thick at the location of the swept interaction, which naturally leads to a large inception zone (see Ref. 7). The dimensional limits of the hypersonic test models used so far have thus precluded the taking of data outside the inception zone.

## Conclusions

This experimental study demonstrates a novel heat transfer technique for high-speed, near-adiabatic wind tunnel testing. A foil heater generates a uniform heat flux over a flat plate

15

surface and miniature thin-film-resistance sensors mounted on it are used to measure the local surface temperature. The heat convection equation is then solved for the heat transfer distribution, yielding a total uncertainty of about ±10%. The novelty of this technique lies in the use of resistance heating rather than cooling for high-speed flows, the microlithographic fabrication of the sensors, and the fact that the adiabatic wall temperature is measured rather than simply assumed to be constant. (However, results show that the adiabatic wall temperature does not vary appreciably in the present experiments.)

The equilibrium turbulent boundary-layer on the flat plate is subjected to impingement by swept planar shock waves generated by a sharp fin. Five different interactions with fin angles ranging from 10° to 20° at freestream Mach numbers of 3.0 and 4.0 produce a variety of interaction strengths from weak to very strong. The heat transfer results show a monotonic rise to a strong peak associated with the primary flow attachment line. The peak heating level varies from 2 to 5 times that of the flat plate over the range of interaction strengths studied.

These data can serve as a "benchmark" for CFD code validation and turbulence modeling. Accordingly, the data are compared with the results of numerical Navier-Stokes solutions which employ a k-ε turbulence model. The overall ability of the computations to predict the data is judged to be good.

Finally, a simple quasiconcial correlation for the peak heat transfer in such fin interactions is suggested. This correlation demonstrates that peak heating is simply proportional to the interaction strength as expressed by the Mach number normal to the swept shock wave. The correlation is effective outside the interaction inception zone which occurs in the vicinity of the fin leading edge.

## Resulting Publications

Lee, Yeol "Heat Transfer Measurements In Swept Shock Wave/Turbulent Boundary-Layer Interactions", Ph.D. Thesis, Pennsylvania State University, Department of Mechanical Engineering, 1992.

Lee, Y. and Settles, G.S. "Heat Transfer Measurements and CFD Comparison of Swept Shcok Wave/Boundary-layer Interactions," AIAA/ASE/ASME/ASEE 28th Joint Propulsion Conference and Exhibit, Nashville, TN, July 6-8, 1992. *Also submitted for publication in AIAA Journal.*

## References

1) Horstman, C. C., "Computation of Sharp-Fin-Induced Shock Wave/-Turbulent Boundary-Layer Interactions," *AIAA Journal*, Vol. 24, No. 9, Sept. 1986, pp. 1433-1440.

2) Knight, D. D., "A Hybrid Explicit-Implicit Numerical Algorithm for the Three-Dimensional Compressible Navier-Stokes Equations," *AIAA Journal*, Vol. 22, No. 8, Aug. 1984, pp. 1056-1063.

3) Knight, D. D., "Calculation of Three-Dimensional Shock/Turbulent Boundary-Layer Interaction Generated by a Sharp Fin," *AIAA Journal*, Vol. 23, No. 12, Dec. 1985, pp. 1885-1891.

4) Knight, D. D. and Badekas, D., "On the Quasi-Conical Flowfield Structure of the Swept Shock Wave-Turbulent Boundary Layer Interaction," AIAA Paper 91-1759, June 1991.

5) Knight, D., Horstman, C. C., and Settles, G. S., "Three Dimensional Shock Wave-Turbulent Boundary Layer Interactions Generated by a Sharp Fin at Mach 4," AIAA Paper 91-0648, Jan. 1991.

6) Settles, G. S., and Dolling, D. S., "Swept Shock Wave Boundary-Layer Interactions," in *AIAA Progress in Astronautics and Aeronautics: Tactical Missile Aerodynamics*, edited by M. Hemsch and J. Nielsen, Vol. 104, AIAA, New York, 1986, pp. 297-379.

7) Settles, G. S., and Dolling, D. S., "Swept Shock/-Boundary-Layer Interactions - Tutorial and Update," AIAA paper 90-0375, Jan. 1990.

8) Lu, F. K., "Fin Generated Shock-Wave Boundary-Layer Interactions," Ph.D. Dissertation, Mechanical Engineering Dept., Pennsylvania State University, 1988.

9) Kim, K-S., Lee, Y., Alvi, F. S., Settles, G. S., and Horstman, C. C., "Laser Skin Friction Measurements and CFD Comparison of Weak-to-Strong Swept Shock/Boundary Layer Interactions," *AIAA Journal*, Vol. 29, No. 10, Oct. 1991, pp. 1643-1650.

10) Alvi, F. S. and Settles, G. S., "Physical Flowfield Model of the Swept Shock/Boundary-Layer Interaction Flowfield," AIAA Paper 91-1768, June 1991, to be published in *AIAA Journal*.

11) Hsu, J. C. and Settles, G. S., "Holographic Flowfield Density Measurements in Swept Shock Wave/-Boundary-Layer Interactions," AIAA Paper 92-0746, Jan. 1992.

12) Neumann, R. D. and Hayes, J. R., "Introduction to Aerodynamic Heating Analysis of Supersonic Missiles," in *AIAA Progress in Astronautics and Aeronautics: Tactical Missile Aerodynamics*, Vol. 104, AIAA, New York, Sept. 1986, pp. 421-479.

13) Holden, M. S., "Experimental Studies of Quasi-Two-Dimensional and Three-Dimensional Viscous Interaction Regions Induced by Skewed-Shock and Swept-Shock Boundary Layer Interaction," AIAA Paper 84-1677, June 1984.

14) Hayashi, M., Sakurai, A., Aso, S., "Measurements of Heat-Transfer Coefficients in the Interaction Regions between Oblique Shock Waves and Turbulent Boundary Layers with a Multi-Layered Thin Film Heat Transfer Gage," *Trans. Japan Society Aero. Space Sci.*, Vol. 30, No. 88, Aug. 1987.

15) Rodi, P. E., and Dolling, D. S., "An Experimental/-Computational Study of Sharp Fin Induced Shock Wave/Turbulent Boundary Layer Interactions at Mach 5: Experimental Results," AIAA Paper 92-0749, Jan. 1992.

16) Schultz, D. J., and Jones, T. V., "Heat Transfer Measurements in Short-Duration Hypersonic Facilities," AGARD-AG-165, Feb. 1973.

17) Moody, H. L., and Jechel, K., "Heat Transfer Measurements in Cold Wind Tunnels," AFWAL-TR-81-3176, Sept. 1982.

18) Neumann, R. D., "Aerothermodynamic Instrumentation," AGARD publication in press.

19) Thompson, W. P., "Heat Transfer Gages," *Methods of Experimental Physics: Fluid Dynamics*, Vol. 18B, Academic Press, 1981, pp. 663-685.

20) Epstein, A. H., Guenette, G. R., Norton, R. J. G., and Yuzhang, C., "High-Frequency Response Heat-Flux Gage," *Rev. Sci. Instrum.*, Vol. 57, No. 4, April 1986.

21) Johnson, C. B., Carraway, D. L., Hopson, P., Jr., and Tran, S. Q., "Status of a Specialized Boundary Layer Transition Detection System for Use in the U.S. National Transonic Facility," ICIASF 1987 Record, pp.141-155.

22) Simonich, J. C., and Moffat, R. J., "New Technique for Mapping Heat-Transfer Coefficient Contours," *Rev. Sci. Instrum.*, Vol 53, No. 5, 1982, pp. 678-683.

23) Hippensteele, S. A., Russell, L. M., and Stepka, F. S., "Evaluation of a Method for Heat Transfer Measurements and Thermal Visualization Using a Composite of a Heater Element and Liquid Crystals." *Journal of Heat Transfer*, Vol. 105, 1983, pp. 184-189.

24) Abuaf, N., Urbaetis, S. P., and Palmer, O. F., "Convection Thermography" Technical Report No. 85CRD168, General Electric Co., Sept. 1985.

25) Eibeck, P. A., and Eaton, J. K., "An Experimental Investigation of the Heat Transfer Effects of a Longitudinal Vortex Embedded in a Turbulent Boundary Layer," Report MD-48, Thermosciences Division, Dept. of Mechanical Engineering, Stanford University, November 1985.

26) Lee, Y., "Heat Transfer Measurements in Swept Shock Wave/Turbulent Boundary-Layer Interactions," Ph.D. Dissertation, Mechanical Engineering Dept., Penn State University, June 1992.

27) Johnson, C. B., and Adcock, J. B., "Measurement of Recovery Temperature on an Airfoil in the Langley 0.3m Transonic Cryogenic Wind Tunnel," AIAA Paper 81-1062, June 1981.

28) Mack, L. M., "An Experimental Investigation of the Temperature Recovery Factor", Report No. 20-80, Jet Propulsion Laboratory, California Institute of Technology, Aug. 1954.

29) Stalder, J. R., Rubesin, M. W., Tendeland, T., "A Determination of the Laminar-, Transitional-, and Turbulent Boundary Layer Temperature Recovery Factors on a Flat Plate in Supersonic Flow," NACA TN 2077, June 1950.

30) Coleman, H. W. and Steele W. G., *Experimentation and Uncertainty Analysis for Engineers*, John Wiley & Sons, 1989.

31) Settles, G. S., Horstman, C. C., and McKenzie, T. M., "Flowfield Scaling of a Swept Compression Corner Interaction - A Comparison of Experiment and Computation," AIAA Paper 84-0096, Jan. 1984.

32) Jones, W. P., and Launder, B. E., "The Prediction of Laminarization with a Two-Equation Model of Turbulence," *International Journal of Heat and Mass Transfer*, Vol. 15, Feb. 1972, pp. 301-314.

33) Knight, D. D., Horstman, C. C., Shapey, B., and Bogdonoff, S. M., "Structure of Supersonic Flow Past a Sharp Fin," *AIAA Journal*, Vol. 25, No. 10, 1987, pp. 1331-1337.

34) Wilcox, D. C., "Program EDDYBL User's Guide," DCW Industries Report DCW-R-NC-04, Nov. 1988.

35) Law, C. H., "3-D Shock Wave-Turbulent Boundary Layer Interactions at Mach 6," USAF ARL TR 75-0191, 1974. (See also: Christophel, R.G., Rockwell, W.A. and Neumann, R.D., "Tabulated Mach 6 3-D Shock Wave-Turbulent Boundary Layer Interaction Heat Transfer Data (Supplement)," AFFDL-TM-74-212-FXG-Supplement, 1975.)

36) Oskam, B., Vas, I. E., and Bogdonoff, S.M., "Oblique Shock Wave/-Turbulent Boundary Layer Interactions in Three Dimensions at Mach 3, Part 2," AFFDL-TR-76- 48, Part II, 1976.

37) Kussoy, M. I., and Horstman, K. C., "Documentation of Two- and Three-Dimensional Shock-Wave-/Turbulent-Boundary-Layer Interaction Flows at Mach 8.2," NASA TM 103838, May 1991.
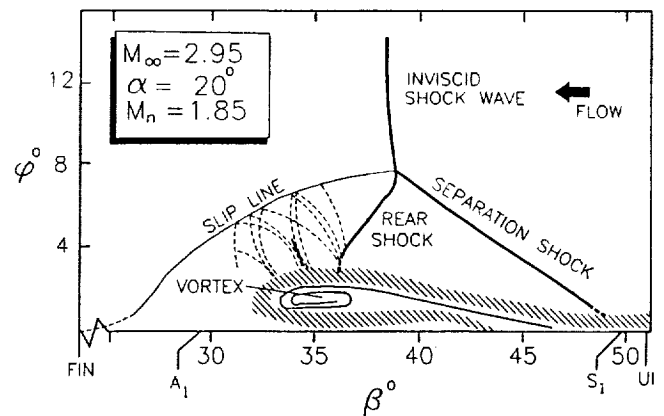
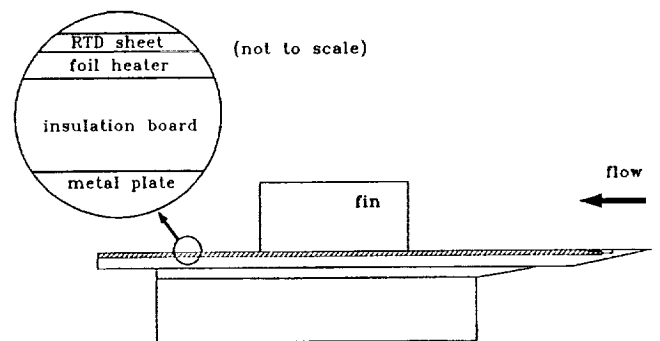Fig. 2 - Map of Conical Flowfield Structure (Ref. 10).



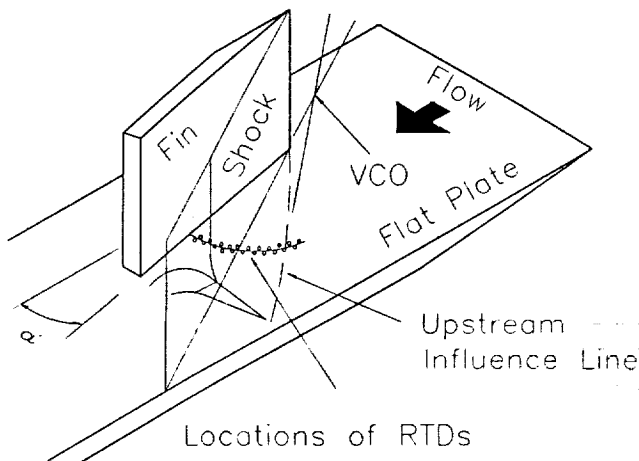Fig. 3 - Sketch of Multilayer Construction of Flat Plate.
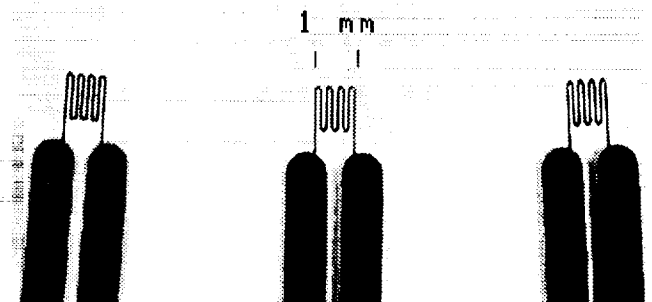


Fig. 1 - Sketch of Test Geometry.



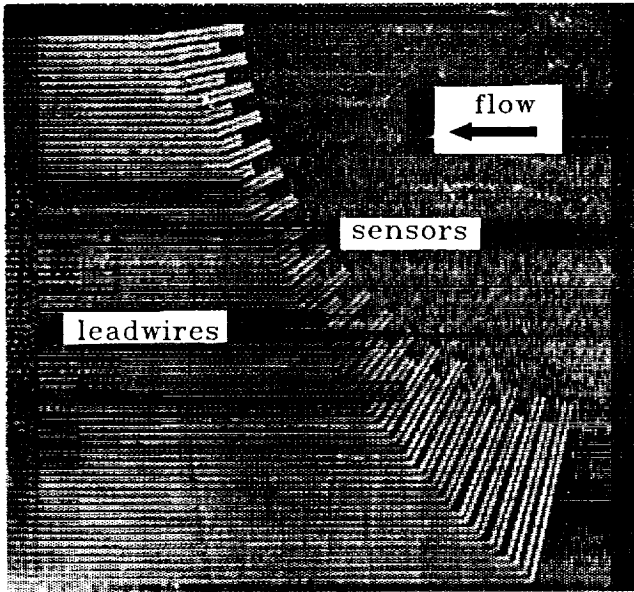Fig. 4 - Magnified Image of RTD Sensors.

Fig. 5 - Image of 37 RTD Sensors Installed on Plate.
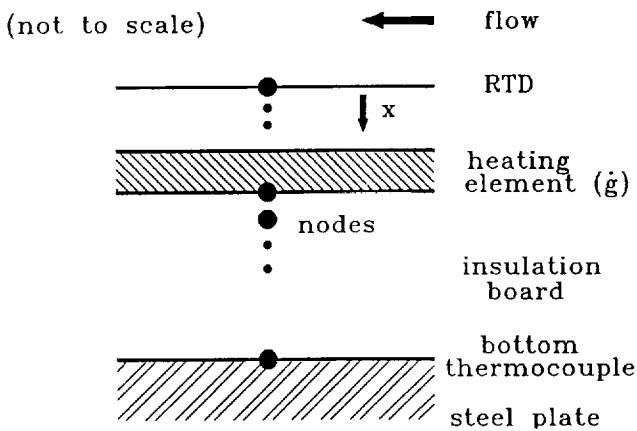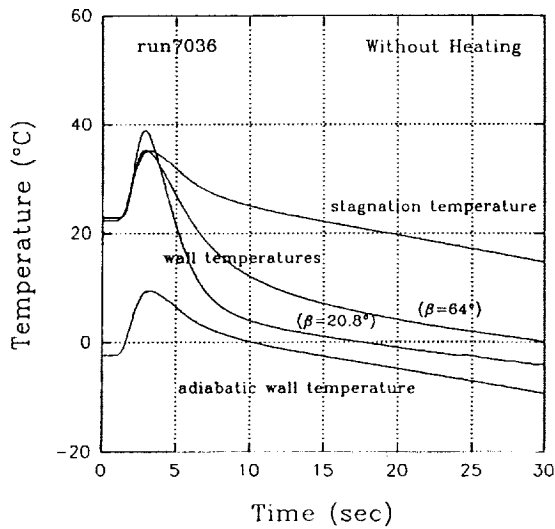


Fig. 6 - Diagram for Computation of Conduction Loss.



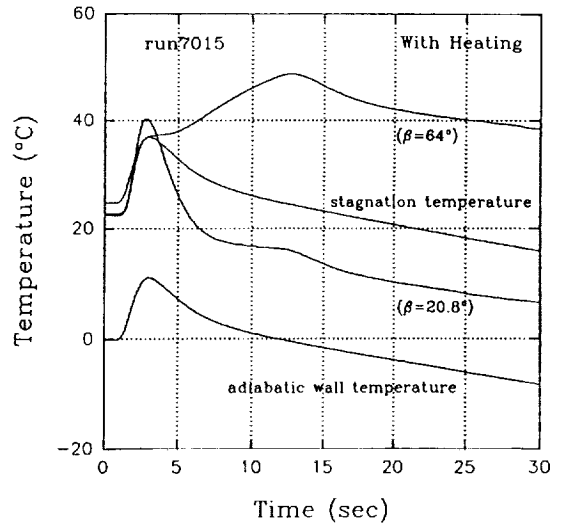Fig. 7 - Temperature Variations Without Heating
(Mach 4, $\alpha$ = 16°).



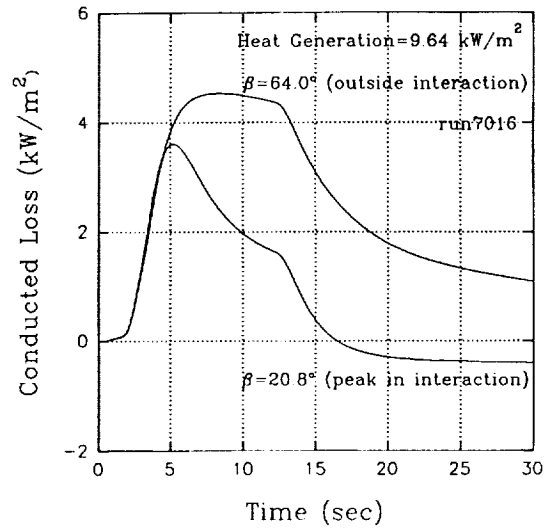Fig. 8 - Temperature Variations With Heating
(Mach 4, $\alpha$ = 16°).



Fig. 9 - Comparison of Conduction Loss Calculation
(Mach 4, $\alpha$ = 16°).



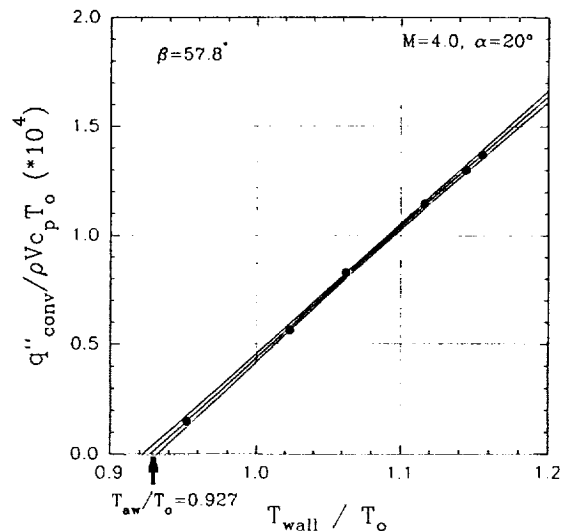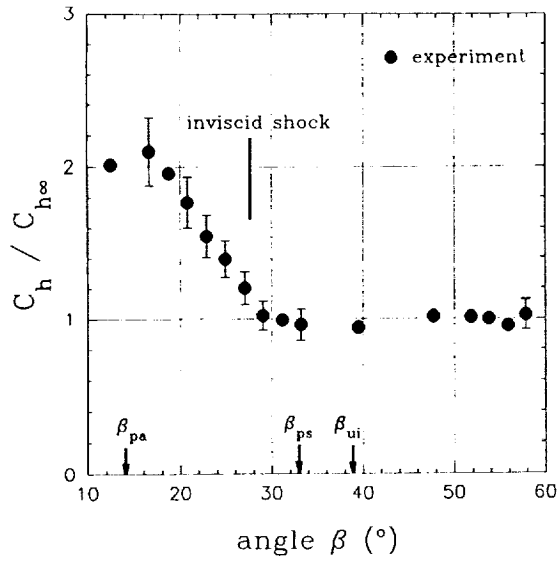Fig. 10 - Example Determination of Adiabatic Wall Temp.

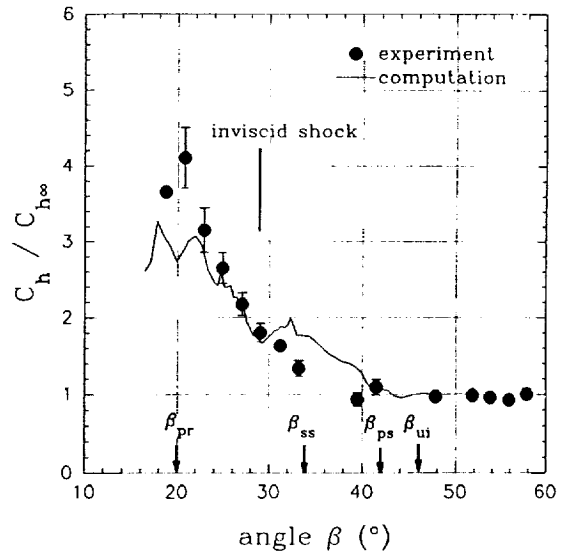Fig. 11 - $C_h/C_{h\infty}$ vs. $\beta$ for Mach 3, $\alpha = 10°$.



Fig. 12 - $C_h/C_{h\infty}$ vs. $\beta$ for Mach 3, $\alpha = 16°$.



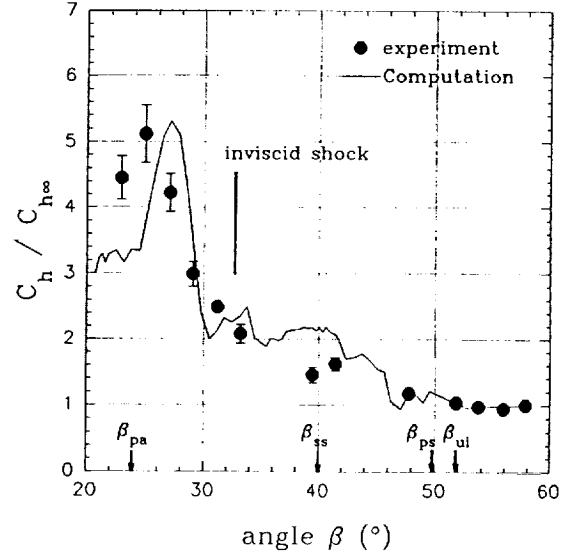Fig. 13 - $C_h/C_{h\infty}$ vs. $\beta$ for Mach 3, $\alpha = 20°$.



Fig. 14 - $C_h/C_{h\infty}$ vs. $\beta$ for Mach 4, $\alpha = 16°$.
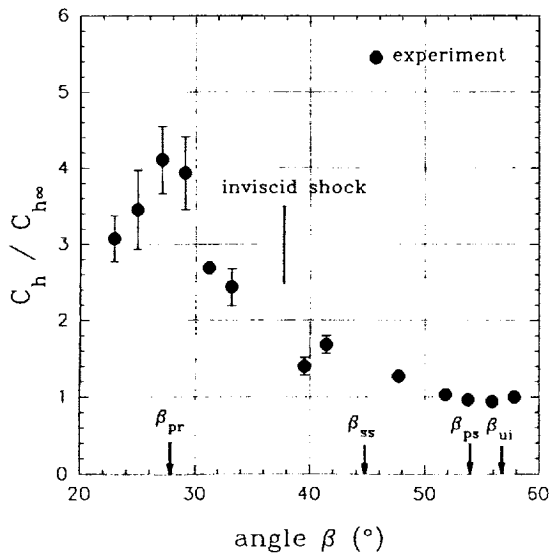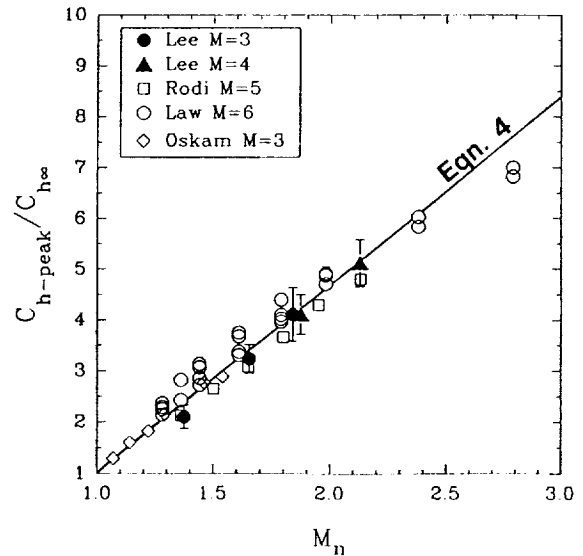


Fig. 15 - $C_h/C_{h\infty}$ vs. $\beta$ for Mach 4, $\alpha = 20°$.



Fig. 16 - New Peak Heating Correlation.